JOURNAL OF VIROLOGY, May 2006, p. 4557–4569 Vol. 80, No. 9
0022-538X/06/$08.00+0 doi:10.1128/JVI.80.9.4557–4569.2006

Retrovirus-Induced Oxidative Stress with Neuroimmunodegeneration Is Suppressed by Antioxidant Treatment with a Refined Monosodium α-Luminol (Galavit)

Yuhong Jiang, Virginia L. Scofield, Mingshan Yan, Wenan Qiang,† Na Liu, Amy J. Reid, William S. Lynn, and Paul K. Y. Wong*

The University of Texas M. D. Anderson Cancer Center, Science Park-Research Division, Smithville, Texas 78957

Received 16 November 2005/Accepted 6 February 2006

Oxidative stress is involved in many human neuroimmunodegenerative diseases, including human immunodeficiency virus disease/AIDS. The retrovirus *ts*1, a mutant of Moloney murine leukemia virus, causes oxidative stress and progressive neuro- and immunopathology in mice infected soon after birth. These pathological changes include spongiform neurodegeneration, astrogliosis, thymic atrophy, and T-cell depletion. Astrocytes and thymocytes are directly infected and killed by *ts*1. Neurons are not infected, but they also die, most likely as an indirect result of local glial infection. Cytopathic effects of *ts*1 infection in cultured astrocytes are associated with accumulation of the viral envelope precursor protein gPr80^{env} in the endoplasmic reticulum (ER), which triggers ER stress and oxidative stress. We have reported (i) that activation of the Nrf2 transcription factor and upregulation of antioxidative defenses occurs in astrocytes infected with *ts*1 in vitro and (ii) that some *ts*1-infected astrocytes survive infection by mobilization of these pathways. Here, we show that treatment with a refined monosodium α-luminol (Galavit; GVT) suppresses oxidative stress and Nrf2 activation in cultured *ts*1-infected astrocytes. GVT treatment also inhibits the development of spongiform encephalopathy and gliosis in the central nervous system (CNS) in *ts*1-infected mice, preserves normal cytoarchitecture in the thymus, and delays paralysis, thymic atrophy, wasting, and death. GVT treatment of infected mice reduces *ts*1-induced oxidative stress, cell death, and pathogenesis in both the CNS and thymus of treated animals. These studies suggest that oxidative stress mediates *ts*1-induced neurodegeneration and T-cell loss.

The retrovirus *ts*1, a mutant of Moloney murine leukemia virus (MoMuLV), induces a progressive neuroimmunodegenerative syndrome in susceptible mice infected as neonates. This syndrome is characterized by tremor, hindlimb paralysis, immunodeficiency, wasting, and death by 30 to 50 days postinfection (p.i.) (14, 34, 63, 66). The *ts*1 virus infects T cells, endothelial cells, astrocytes, microglia, and oligodendrocytes, but like human immunodeficiency virus (HIV), it does not replicate in neurons (18, 55, 56, 69). T-cell depletion, thymic atrophy, spongiform vacuolation in the central nervous system (CNS) with local astrogliosis, and neuronal depletion are the major histopathological signs of *ts*1 infection (18, 57, 63).

Thymocytes isolated from mice infected with *ts*1 rapidly die by apoptosis (49, 67). However, only about 40% of astrocytes infected with *ts*1 in culture die, while the remaining astrocytes survive and continue to proliferate (28, 46, 50). In infected mice, likewise, some *ts*1-infected astrocytes die while others are activated and accumulate in astrogliotic foci in the spongiform lesions (56, 71). Since neurons are not infected, they apparently die as an indirect result of local glial infection (34, 56, 57).

Oxidative stress occurs in cells when the production of reactive oxygen species (ROS) exceeds intracellular antioxidant defenses (5). At low concentrations, ROS can stimulate cell proliferation (4, 27), but at higher concentrations, they damage cells by oxidizing proteins, DNA, and lipids (20, 32) or by initiating apoptotic pathways (12). Oxidative stress has been implicated in the neuropathogeneses of many diseases, such as HIV-associated dementia (17, 36, 38, 39, 60), Alzheimer's disease (8, 37, 51, 52), and ataxia telangiectasia (3, 6, 10, 21, 31).

Many viruses, including retroviruses, initiate oxidative stress in infected cells. Oxidative stress in cells is accompanied by accumulation of ROS, oxidant damage, and depletion of reduced thiols (9, 13, 44, 45, 47, 61). The source(s) of ROS in virus-infected cells is unclear. In humans, infection with HIV type 1 is associated with elevated serum levels of products of lipid peroxidation, including malondialdehyde (MDA) (16, 53). These patients also show decreased plasma levels of the reduced thiols glutathione (GSH) and cysteine, both of which participate in antioxidant defenses (7, 15, 16).

Infection of thymocytes and astrocytes with *ts*1 in vitro causes both intracellular accumulation of gPr80^{env} (18, 50, 58, 66) and overproduction of ROS, with depletion of GSH and cysteine. We have shown previously that gPr80^{env} accumulation in the endoplasmic reticulum (ER) of *ts*1-infected cells causes ER stress, with release of calcium (Ca^{2+}) from ER stores (24, 29). This in turn results in mitochondrial stress, resulting from mitochondrial membrane permeabilization, uncoupling of the respiratory chain, and cytochrome *c* release, followed by mitochondrial stress (23, 25, 29, 43, 54).

In cells undergoing oxidative stress, the redox-sensitive transcription factor NF-E2-related factor 2 (Nrf2) is upregulated

* Corresponding author. Mailing address: Department of Carcinogenesis, The University of Texas M. D. Anderson Cancer Center, Science Park-Research Division, P.O. Box 389, Smithville, TX 78957. Phone: (512) 237-9456. Fax: (512) 237-2444. E-mail: pkwong@mdanderson.org.

† Present address: Department of Molecular Pharmacology and Biological Chemistry, Northwestern University Feinberg School of Medicine, Chicago, IL 60611.

and translocated to the nucleus, thereby upregulating the expression of GSH synthesis-related genes (22, 26). We have reported that the Nrf2 antioxidative response pathway is activated in astrocyte cultures infected with *ts*1 (45) and that some cells in such cultures survive infection as a consequence of these defenses (46).

We have also shown that treatment of *ts*1-infected mice with the antioxidant *N*-acetylcysteine (NAC) delays the onset of hindlimb paralysis and delays thymic atrophy (35). Similar partial therapeutic results were observed in *ts*1-infected mice treated with the peroxisome proliferator phenylbutyric acid (PBA), which upregulates production of the H_2O_2 scavenger catalase (30).

We show here that a refined monosodium α-luminol (Galavit; GVT) suppresses ROS accumulation and oxidative stress in *ts*1-infected primary astrocyte cultures (PACs). In *ts*1-infected mice, GVT administration suppresses hindlimb paralysis, body wasting, thymic atrophy, and development of spongiform and astrogliotic encephalopathy in the CNS. GVT treatment also reduces lipid peroxidation in the CNS and thymus of infected animals.

In *ts*1-infected mice, GVT treatment prevents cytopathic effects both in the CNS and in the thymus. Although *ts*1 replication continues in the thymus during treatment of infected mice, it is suppressed in the CNS if treatment is begun immediately after infection. However, when GVT treatment is delayed until 10 days p.i., allowing initial viral replication in the CNS, neuroprotection occurs without effects on the viral titer. We conclude that GVT suppresses virus replication and virus-induced cytopathology in the CNS by reducing oxidant stress, rather than by way of direct antiviral effects of the drug. Similarly, GVT protection of the thymus, which occurs while virus is replicating there, indicates that cytopathic effects of *ts*1 in this location are also caused by oxidative stress resulting from infection, rather than by the viral load per se.

MATERIALS AND METHODS

Cells and cell culture. TB cells, a thymus-bone marrow cell line, were derived from CFW/D mice (2) using a procedure described previously (70). 15F cells, cultured from a murine untransformed, sarcoma-positive, leukemia-negative cell line, were derived from TB cells infected with Moloney sarcoma virus (1, 65). All these cell lines were grown in Dulbecco's modified Eagle's medium (DMEM) supplemented with 10% fetal bovine serum, 100 units/ml penicillin, 100 μg/ml streptomycin in a 37°C incubator with 5% CO_2 in air. PACs were isolated from 1- to 2-day-old FVB/N mice as described previously (50). Briefly, the cells were seeded into poly-L-lysine-coated flasks and grown in DMEM–F-12 medium supplemented with 10% fetal bovine serum, 100 units/ml penicillin, 100 μg/ml streptomycin, and 2.5 μg/ml fungizone, and the medium was changed every 3 days. After reaching confluence, the cells were passaged four or five times and used before reaching confluence again. At this point, more than 99% of the cells in the cultures were positive for the astrocyte-specific glial fibrillary acid protein (GFAP) marker (50).

Virus. The *ts*1 virus, a mutant of MoMuLV, and the parent strain MoMuLV-TB, or wild-type (WT) virus, was propagated in TB cells and titered on 15F cells, as previously described (65).

Intracellular ROS assay. Intracellular ROS were measured with 5-(and-6)-chloromethyl-2′,7′-dichlorodihydrofluorescein diacetate acetyl ester (CM-H_2DCFDA) (Molecular Probes, Eugene, OR), as described previously (45). Briefly, half of each of the mock-infected and virus-infected PACs were treated with either NAC or GVT. As a positive control representing PACs under induced oxidative stress, some cultures of uninfected PACs were exposed to culture medium containing 88 μM H_2O_2. After this step, all the cell cultures were loaded with CM-H_2DCFDA at a concentration of 10 μM and incubated at 37°C for 30 min. The dye-loaded cells were then harvested, and their forward and side scatter fluorescences were determined using a Coulter Epics Elite software program, version 4.02 (45).

Western blotting analysis. Western blotting analysis of cell and tissue proteins was performed as described previously (45, 46). The antibodies used in Western blotting analysis included anti-Nrf2 (Santa Cruz Biotechnology, Santa Cruz, CA), anti-glutathione peroxidase (GPx) (Chemicon International, Temecula, CA), and anti-xCT. xCT is one of two subunits of the cell membrane cystine-glutamate antiporter system X_c^-. Anti-xCT was prepared in our laboratory against the synthetic peptide SMGDQEPPGQEKVVLKKKIT (amino acids 26 to 45 of the mouse xCT antiporter).

The net intensities of protein bands of interest were determined by densitometric analysis of autoradiographs with a Kodak (Rochester, NY) Digital Science Image Station 440 CF and Kodak 1D Image Analysis software. Band intensities were then normalized to β-actin intensities and compared for differences between experimental and control conditions. All Western blotting results were replicated in three independent experiments.

***ts*1 infection and GVT treatment of cultured astrocytes.** PACs were isolated from the cerebral cortexes of 1- to 2-day-old mice and seeded into six-well plates. On the second day of culture, all cells were treated with 3 μg/ml Polybrene in DMEM–F-12 for 1 h and then treated either with virus diluent alone (control uninfected cells) or with *ts*1 supernatant (from infected TB cells) at a multiplicity of infection of 15 for 40 min at 34°C. At this multiplicity of infection, more than 99% of the cells are infected by virus from the original inoculum. The uninfected and infected cultures were then washed and divided into groups that received no treatment (vehicle alone), NAC treatment, or GVT treatment at different concentrations. At 48 h p.i., culture supernatants were aspirated and stored at −80°C for later measurement of their contents of *ts*1 virus (65). At the same time, the cells from these cultures were trypsinized, resuspended, and stained with trypan blue for 5 min, and living and dead cells were counted with a hemocytometer.

Mice, infection, and drug treatment. FVB/N mice were obtained from Taconic Farms (Germantown, NY). Breeding pairs were housed in sterilized microisolator cages and supplied with autoclaved feed and water ad libitum. The microisolators were kept in an environmentally controlled isolation room. For *ts*1 or WT infection, 4-day-old mice were inoculated intraperitoneally with 0.1 ml of vehicle (mock infection) or with 0.1 ml of a *ts*1 or WT virus suspension containing 2×10^7 infectious units (IU)/ml of *ts*1 or 2.4×10^7 IU/ml of the WT.

Before testing for a therapeutic effect of GVT in *ts*1-infected mice, we first tested GVT for its toxicity in uninfected FVB/N animals at either of the two treatment dosages used in this study (125 mg/kg of body weight/day or 250 mg/kg of body weight/day). Three groups of FVB/N mice were treated daily by intraperitoneal injection, beginning at 6 days after birth, with 0.9% normal saline (untreated controls), 125 mg/kg of body weight/day of GVT or 250 mg/kg of body weight/day of GVT for 30 days. Starting from the first day of injection, the body weights of all animals in each group were recorded and averaged at specified time points.

To test GVT for its ability to ameliorate *ts*1 disease, animals from the control, *ts*1-infected, and WT virus-infected groups of mice were divided again into two groups each at 2 days p.i., with one group receiving 0.9% normal saline and the other receiving freshly prepared GVT (250 mg/kg of body weight/day; kindly provided by Bach Pharma, Inc., North Andover, MA) delivered intraperitoneally for 5 continuous days per week, followed by 2 resting days, for 50 days. A second experiment was set up in which the GVT dose was half of the original dose (125 mg/kg of body weight/day), and treatment lasted for 100 days. Finally, a third set of animals was infected with *ts*1, with some animals treated with vehicle only and others treated with GVT (250 mg/kg of body weight/day), with both treatments beginning at 10 days p.i. rather than immediately after infection. Some of this third set of animals were sacrificed at 30 days p.i. for *ts*1 titer determinations, while others were followed for the construction of survival curves (treatment stopped at 50 days p.i.).

Mice from all groups were checked daily for clinical signs of disease and sacrificed when moribund and paralyzed. Parallel experiments were done for tissue virus titer assays, thymus weight, and immunohistochemistry studies. The brainstems, spinal cords, and thymi were removed at 10, 20, 30, and 80 days p.i., snap-frozen in liquid nitrogen, and stored at −80°C until they were used. Alternatively, tissues were snap-frozen in liquid nitrogen in optimal cutting temperature (OCT) embedding medium (Sakura Finetek, Inc., Torrance, CA) for frozen-section immunohistochemistry or were incubated in 10% formalin for histological analysis. All animal procedures were performed according to protocols approved by The University of Texas M. D. Anderson Cancer Center Institutional Animal Care and Use Committee.

Virus detection and quantitation in tissues. Frozen brainstem, spinal cord, and thymus tissues were weighed and then homogenized (40 strokes) (Kontes Glass Co., Vineland, NJ) in 2 ml ice-cold basal DMEM (11). Cell debris was

removed by filtration through a 0.45-μm syringe filter (Pall Corporation, Ann Arbor, MI). The titers (IU/ml) of *ts*1 in these lysates were determined using a modified 15F assay (65), in which *ts*1 in each tissue was measured using the following formula: [volume of sample (2 ml) × virus titer in the sample]/weight of tissue (g). The titer of virus was taken as the average titer from three to six mice.

Histopathology and immunohistochemistry. Formalin-fixed, paraffin-embedded tissues from control uninfected, *ts*1-infected untreated, and *ts*1-infected GVT-treated mice were cut into 5-μm-thick sections, attached to slides, deparaffinized, rehydrated, and stained with hematoxylin and eosin (HE) for histopathological analysis. For GFAP immunostaining of paraffin sections, endogenous peroxidase activity was blocked by incubation of the slides in 3% H_2O_2 for 10 min. After antigen retrieval (heating in a microwave oven), the slides were incubated for 30 min in 10% goat serum in phosphate-buffered saline, followed by washing and incubation for 30 min (at room temperature) in rabbit anti-mouse GFAP primary antibody (DAKO, Santa Barbara, CA). After incubation, the sections were washed with phosphate-buffered saline and then incubated in horseradish peroxidase-conjugated anti-rabbit immunoglobulin G (IgG) (DAKO) for 30 min at room temperature.

For gp70 and MDA staining, serial 5-μm-thick frozen sections were cut from OCT-embedded blocks, placed on microscope slides, and kept at −80°C. One of every five sections was stained with HE. The other frozen sections were thawed at room temperature for 30 min, fixed in ice-cold acetone for 5 min, washed, and incubated overnight at 4°C with goat anti-gp70 (Microbiology Associates, Burlingame, CA) and with rabbit anti-MDA antibody (Alpha Diagnostics, San Antonio, TX). Anti-gp70 and anti-MDA antibody binding was detected by incubation of the slides in fluorescein isothiocyanate-conjugated donkey anti-goat IgG F(ab′)2 (Jackson Laboratories, West Grove, PA) mixed with Texas Red-conjugated anti-rabbit IgG (Jackson Laboratories, West Grove, PA). After incubation in the secondary reagents and washing, the sections were mounted in Vectastain mounting medium (Vector Laboratories, Burlingame, CA) for viewing under an Olympus BX40 fluorescence microscope. Control sections were incubated in the presence of affinity-purified goat and rabbit IgG, followed by secondary antibodies, or in secondary antibodies alone without primary reagents. No specific binding was observed on these control sections (data not shown).

[^{3}H]thymidine incorporation into DNA. Thymocytes were isolated by a routine method (48, 67, 68). Single-cell suspensions of thymocytes were incubated in 96-well plastic tissue culture plates at 37°C in the presence of 0.5 μCi of [^{3}H]thymidine (Amersham Pharmacia Biotech, Piscataway, NJ) per well. After 4 h, the cells were harvested, and [^{3}H]thymidine incorporation into DNA was measured with a scintillation counter (Packard, Meriden, CT). The results were expressed as mean counts per minute ± standard deviation in triplicate cultures.

Statistical analysis. Quantitative differences between groups were compared for statistical significance by analysis of variance or Student's *t* test. Survival data were handled using Kaplan-Meier analysis. *P* values of <0.05 were considered statistically significant.

RESULTS

GVT is not toxic to FVB/N mice in the test doses used. The chemical structure of GVT, a refined monosodium α-luminol (monosodium 5-amino-2-3-dihydro-1-4-phthalazine dione), is shown in Fig. 1A. This drug has anti-inflammatory effects in humans. Although the acute and chronic toxicities of GVT have been studied extensively by Russian scientists, the compound was not available in the United States until recently (40).

Before testing of GVT for its ability to protect *ts*1-infected cells and animals, we first conducted experiments to determine whether GVT is toxic to FVB/N mice at the different treatment dosages to be used. Figure 1B shows that body weight gains were identical in the two treated groups of mice versus the age-matched controls at all time points in the experiment. The treated mice in Fig. 1B were also followed closely for any differences from the untreated controls in their skin texture, hair density and texture, and behavior, as well as food and water intake, with all groups being similar for these parameters throughout the 30-day experimental period (data not shown). We also performed histological examinations of sections from the brainstem, spinal cord, thymus, and spleen from the three

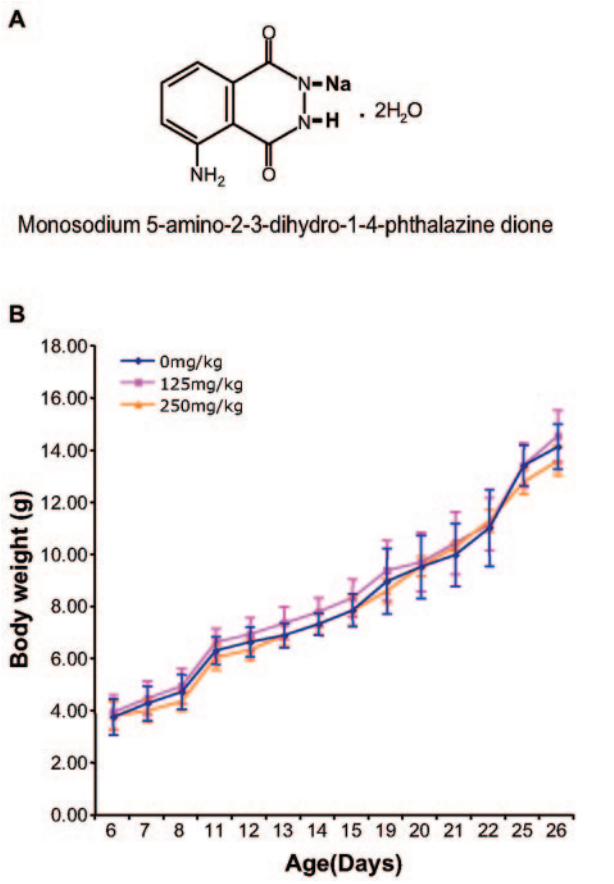

FIG. 1. Chemical structure of GVT and lack of GVT toxicity in mice at therapeutic doses. (A) GVT structure. (B) For studies of the effect of GVT on the growth of FVB/N mice, 6-day-old FVB/N mouse pups were divided into three groups, and the different groups were given intaperitoneal injections of normal saline, GVT in normal saline (250 mg/kg of body weight/day), or GVT in normal saline (125 mg/kg of body weight/day), with injections given 5 days per week. At each time point, six mice from each group were weighed. The graph shows the mean body weight ± standard deviation for each group at each time point. All animals were also observed daily for behavioral and clinical manifestations of drug toxicity.

groups and detected no differences in histomorphology between tissues from treated and untreated mice over the 26-day period (data not shown). We conclude that GVT treatment by itself is nontoxic to FVB/N mice at the dosages used for treatment in this study.

GVT treatment reduces ROS accumulation in *ts*1-infected astrocytes. We have shown previously that in vitro *ts*1 infection of PACs, or C1 astrocytic cells, causes intracellular ROS accumulation, followed by cell death, in approximately 40% of the astrocyte population (45). To determine whether *ts*1-induced ROS accumulation and cell death could be countered by the antioxidant NAC or GVT, we compared intracellular ROS levels in control uninfected, *ts*1-infected untreated, and *ts*1-infected NAC-treated or *ts*1-infected GVT-treated cells by flow cytometry, using the H_2O_2 indicator dye CM-H_2DCFDA (45). As a positive control for oxidatively stressed PACs, one group of uninfected PACs was exposed to 88 μM H_2O_2 before all cells were loaded with 10 μM CM-H_2DCFDA.

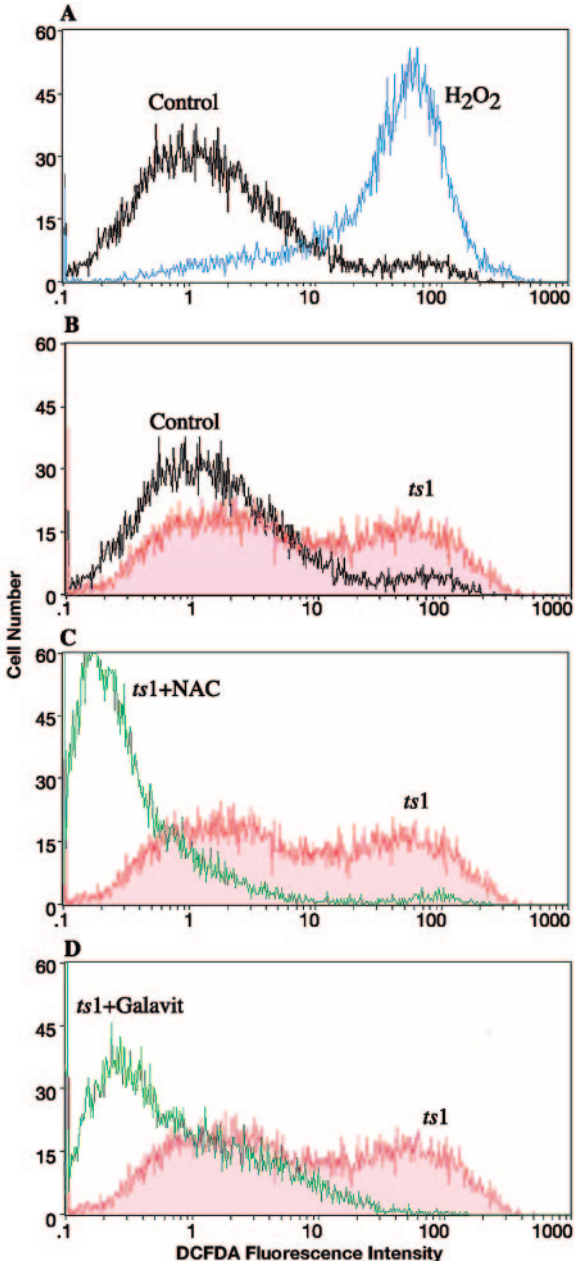

FIG. 2. Intracellular H_2O_2 levels in *ts*1-infected untreated and *ts*1-infected GVT-treated primary astrocyte cultures. Uninfected or infected PACs were untreated, treated with 10 μM GVT, or treated with 5 mM NAC. After being cultured for 48 h, one group of uninfected PACs was pulsed with culture medium containing 88 μM H_2O_2 to serve as a positive control for cells containing elevated H_2O_2. Cells from all of the cultures were then loaded with 10 μM CM-H_2DCFDA for 30 min, followed by flow cytometric measurement of their H_2O_2 contents. (A) FACS histogram of ROS levels in untreated uninfected PACs (black line) versus H_2O_2-treated PACs (blue line). (B) FACS histogram of uninfected PACs (black line) versus *ts*1-infected PACs (red line and red fill). (C) FACS histogram of *ts*1-infected PACs treated with NAC (green line) versus *ts*1-infected PACs left untreated (red line and red fill). (D) FACS histogram of *ts*1-infected PACs treated with GVT (green line) versus *ts*1-infected PACs left untreated (red line and red fill).

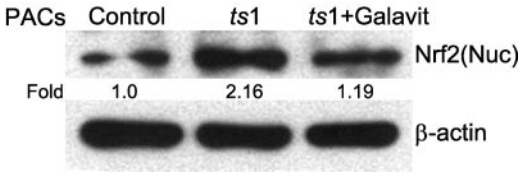

FIG. 3. GVT treatment suppresses Nrf2 nuclear translocation in *ts*1-infected PACs. Uninfected or infected PACs were either left untreated or treated with 100 μM GVT for 48 h, at which time their nuclear proteins were extracted and immunoblotted with antibody to Nrf2. The results are representative of three independent experiments. Band intensities were then normalized to β-actin intensities and compared for differences between experimental and control conditions.

The fluorescence-activated cell sorter (FACS) fluorescence intensity diagrams in Fig. 2A show that, as expected, intracellular H_2O_2 was increased in H_2O_2-treated PACs relative to H_2O_2 in untreated PACs. Figure 2B shows that for PACs infected with *ts*1, intracellular H_2O_2 was also increased over control levels in some (~40%) of the cells, producing a bimodal curve with low-H_2O_2 cells under the left peak and high-H_2O_2 cells under the right peak. *ts*1-induced increases in H_2O_2 were reduced both by NAC (Fig. 2C) and by GVT (Fig. 2D).

GVT suppresses upregulation of Nrf2 in *ts*1-infected PACs. The transcriptional regulator Nrf2 is upregulated and translocated to the nucleus in *ts*1-infected PACs and C1 cells, where it activates the transcription of target genes with antioxidant response element sequence-containing promoters (45). We have also shown that some *ts*1-infected cultured astrocytes can survive *ts*1 infection by mobilizing these defenses (46). To assess the degree to which GVT might affect the activation of Nrf2, we used Western blotting to compare levels of nuclear Nrf2 in uninfected PACs, *ts*1-infected untreated PACs, and *ts*1-infected PACs treated with 100 μM GVT after being cultured for 48 hours p.i. Figure 3 shows that while nuclear levels of Nrf2 were increased in cultured *ts*1-infected PACs by 48 hours p.i., Nrf2 levels in the GVT-treated infected PACs were similar to those of uninfected PACs.

GVT promotes survival in *ts*1-infected mice. *ts*1 infection of PACs or C1 cells results in accumulation of intracellular ROS, leading to oxidative stress in the cells (45). In the CNS, this oxidative stress is likely to be the ultimate cause of death for neurons, although neurons are not infected by *ts*1. Before we knew about the antioxidative properties of GVT, we had already tested NAC (35) and PBA (30) as candidate treatments for delaying neurodegeneration in *ts*1-infected mice. While both drugs significantly delayed body wasting, and although both drugs lengthened the average time from infection to onset of paralysis, neither one prevented the eventual appearance of these symptoms, even if treatment was never terminated. In addition, both NAC and PBA were toxic at therapeutic doses, while effective doses of GVT are not (Fig. 1B). Since GVT also protects *ts*1-infected cultured PACs from oxidative stress at lower doses than does NAC (Fig. 2), we hypothesized that the drug might be more effective than NAC (35) or PBA (30) for protection of *ts*1-infected mice against the neurodegeneration and thymic atrophy/immunosuppression that follow infection.

To test this hypothesis, we randomly divided uninfected and *ts*1-infected FVB/N newborns into two groups, one of which

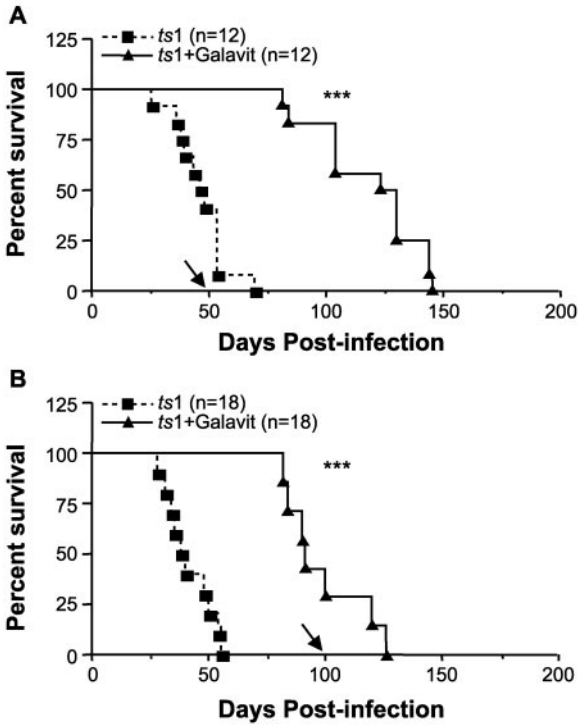

FIG. 4. GVT treatment promotes survival in *ts*1-infected mice. (A) Twenty-four mice were infected with *ts*1 4 days after birth and then were divided into two groups. Twelve received intraperitoneal injections of GVT, at 250 mg/kg of body weight/day, and the other 12 received the same volume of 0.9% normal saline (infected controls) using the same route. Treatment was continued for 5 days/week and stopped at 50 days p.i. (arrow). At that time, 83% of the mice in the untreated infected control group had died, but all of the GVT-treated mice were alive. ***, $P < 0.001$. (B) Thirty-six mice were infected with *ts*1 4 days after birth and then were divided into two groups. Eighteen mice received intraperitoneal injections of GVT, at 125 mg/kg of body weight/day, and the other 18 received 0.9% normal saline (infected controls) by the same route for 5 days per week. In this experiment, treatment was continued until 100 days p.i. (arrow). As shown, all of the mice in the infected untreated control group had died by 55 days p.i., like the infected untreated control mice in panel A. At that time, all of the GVT-treated mice were alive and healthy. When GVT treatment was stopped at 100 days p.i., however, 78% of the animals in this group had died. ***, $P < 0.001$.

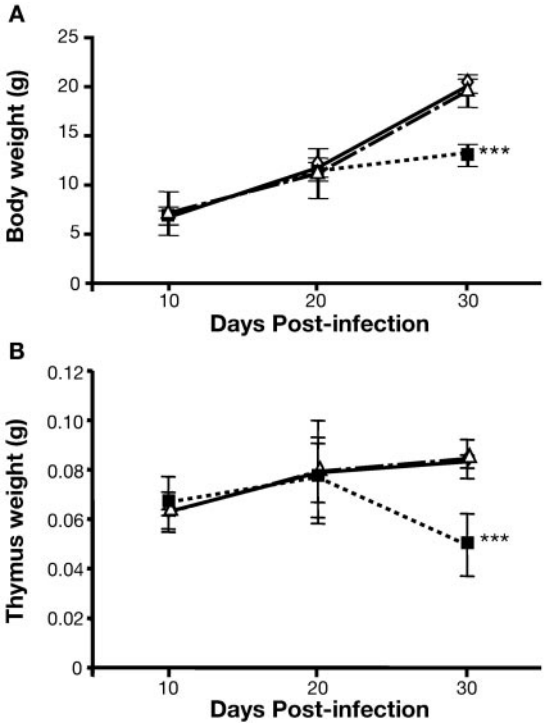

FIG. 5. GVT treatment protects against *ts*1-induced wasting and thymic atrophy. (A) Control uninfected, *ts*1-infected untreated, and *ts*1-infected GVT-treated mice (using the 250-mg/kg/day, 5-day/week regimen) were weighed at 10, 20, and 30 days p.i.. Shown are average body weights, ± standard deviations, for three to six animals from the three different groups at each time point. (B) In a parallel experiment, control uninfected, *ts*1-infected untreated, and *ts*1-infected GVT-treated mice were sacrificed at 10, 20, and 30 days p.i., at which times thymi from three to six mice were removed and weighed. ***, $P < 0.001$. ◇, control; ■, *ts*1; △, *ts*1 plus GVT.

received intraperitoneally injected 0.9% normal saline, with the other receiving the same volume of GVT solution (250 mg/kg of body weight/day), each for 5 days/week. In this experiment, treatment was stopped at 50 days p.i. By that time, 83% of the mice in the untreated infected group had died (Fig. 4A), and all the surviving mice in this untreated group were paralyzed. Remarkably, none of the GVT-treated infected mice showed wasting or paralysis at this point. However, reemergent virus infection, evidenced by tremor and paralysis, was observed in the treated mice beginning at 80 days p.i. (30 days after the treatment was stopped), and all of the GVT-treated animals had died by 145 days p.i. (Fig. 4A), after developing wasting and paralysis.

In a second experiment, we examined the effects of GVT given at a dosage of 125 mg/kg of body weight/day, but over a longer period (up to 100 days p.i., rather than 50 days p.i.). Figure 4B shows that all of the *ts*1-infected mice in the untreated control group in this experiment, like those in Fig. 4A, had died between 30 and 56 days p.i. In the GVT-treated group from this experiment, however, the first deaths occurred at 84 days p.i., while the drug was still being administered. Under these treatment conditions, 78% of the GVT-treated mice were dead when the treatment was stopped at 100 days p.i. The remaining 22% of GVT-treated mice were still alive and apparently healthy at this time point, but all of these mice died on or before 126 days p.i., after developing wasting and paralysis. These results suggest that protection by GVT is dose dependent. Because the 250-mg/kg dose was the more effective of the two, all subsequent animal experiments were done by this protocol.

GVT delays body wasting and thymic atrophy in *ts*1-infected mice. In *ts*1-infected mice not treated with GVT, tremor is usually evident by 21 days p.i., and the animals develop hindlimb paralysis and show obvious body wasting by 30 to 50 days p.i. (64). By this time, their thymi are atrophied, and their peripheral $CD4^+$ T-cell numbers are significantly reduced relative to those of healthy mice (49, 55, 62). To determine whether GVT prevents body wasting and thymic atrophy in *ts*1-infected mice, we compared the average body weights and thymic weights of control uninfected mice, infected untreated mice, and infected mice treated with GVT. Figure 5A shows

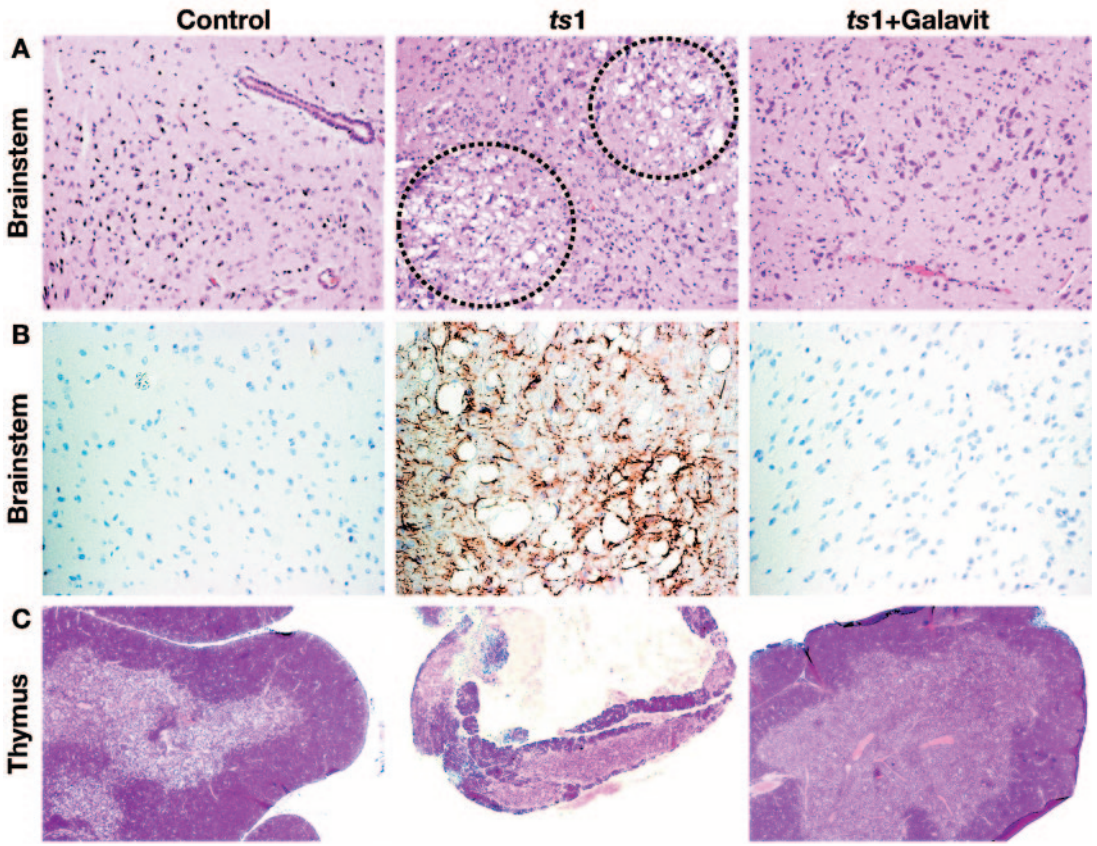

FIG. 6. Effects of GVT on CNS histopathology and thymic cytoarchitecture in *ts*1-infected mice. (A) Paraffin sections of brainstem tissues of normal control (left), *ts*1-infected untreated (middle), and *ts*1-infected GVT-treated (right) mice were cut from brainstems taken from mice sacrificed at 30 days p.i. and stained with HE. Note the typical *ts*1-induced spongiform degeneration (circles) in the brainstem section from the *ts*1-infected untreated mouse (middle). (B) Paraffin sections of brainstem tissues of normal control (left), *ts*1-infected untreated (middle), and *ts*1-infected GVT-treated (right) mice were prepared at 30 days p.i., as described above, and immunostained for the astrocyte marker GFAP. Note that many GFAP-positive astrocytes (brown staining of astrocyte processes) are present in the brainstem section from the *ts*1-infected untreated mouse (middle). (C) The thymus of the *ts*1-infected mouse (middle) also shows dramatic thinning and atrophy and has lost its corticomedullary organization. Magnification, (A) ×200; (B) ×400; (C) ×40.

that while the untreated infected mice in this experiment began to lose weight after 20 days p.i., the GVT-treated mice grew normally, with body weights comparable to those of uninfected mice at all time points. Similarly, Fig. 5B shows that thymic weights increased normally in *ts*1-infected GVT-treated mice, while thymi of untreated infected mice lost weight and became smaller than thymi from control uninfected or GVT-treated mice after 20 days p.i.

GVT suppresses spongiform neurodegeneration, astrogliosis, and thymic lobular collapse in *ts*1-infected mice. As noted above, *ts*1-infected mice develop gliosis and spongiform lesions in the CNS (56, 57), and their thymi degenerate, in association with the development of immunodeficiency and selective loss of peripheral $CD4^+$ cells (49, 62). In the brainstem, spongiform lesions first appear as perivascular and paraventricular spongiform changes, followed by cytoplasmic vacuolation in neuronal and glial cells. This is associated with almost complete neuronal dropout from the brainstem and the cervical and lumbar spinal cord and with the appearance of GFAP-positive astrocytes in and around the spongiform lesions (56, 57). In the thymus, *ts*1-induced histopathology is evident first in cortical thinning, which is followed by complete loss of corticomedullary organization and subsequently by widespread cell death and collapse of the thymic lobules (55, 62).

To determine whether and how GVT might slow the CNS and thymic histopathology that characterizes *ts*1-induced disease, we prepared paraffin-embedded brainstem and thymus tissues from control uninfected, *ts*1-infected untreated, and *ts*1-infected GVT-treated mice sacrificed at 30 days p.i. These sections were then stained either with HE (for general histopathological examination of the brainstem or thymus) or with anti-GFAP (to detect astrogliosis in the brainstem sections). Figure 6A and B show microscopic fields from control uninfected, infected untreated, and infected GVT-treated brainstem sections, from left to right, respectively, and stained with HE (Fig. 6A) or immunostained for GFAP (Fig. 6B). Viewed alongside the sections from control uninfected mice in the left panels of Fig. 6A and B, the sections from *ts*1-infected untreated mice (middle panels of Fig. 6A and B) contained multiple spongiform lesions and showed pronounced localized astrogliosis in association with these lesions. By contrast, neither spongiform lesions nor astrogliosis were evident in brainstem sections from *ts*1-infected GVT-treated mice (Fig. 6A and B, right panels).

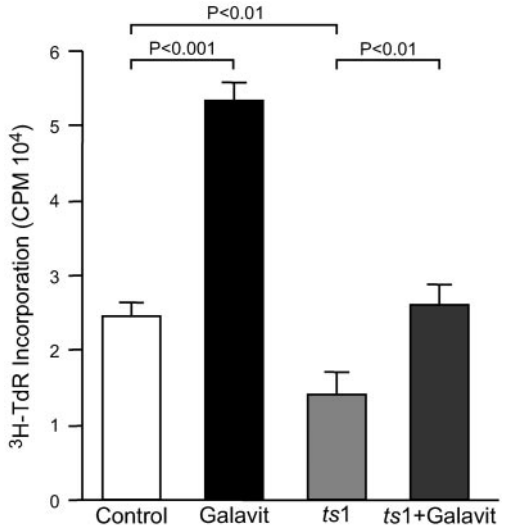

FIG. 7. GVT treatment increases DNA synthesis in thymocytes from *ts*1-infected mice. Thymocytes freshly isolated from uninfected, uninfected GVT-treated, *ts*1-infected untreated, and *ts*1-infected GVT-treated mice at 30 days p.i. were cultured in 96-well plates at 37°C for 4 h in the presence of 0.5 μCi of [^{3}H]thymidine. After 4 h, the cells were harvested and [^{3}H]thymidine incorporation into DNA was measured with a scintillation counter. The results are expressed as mean counts per minute plus standard deviation in triplicate cultures.

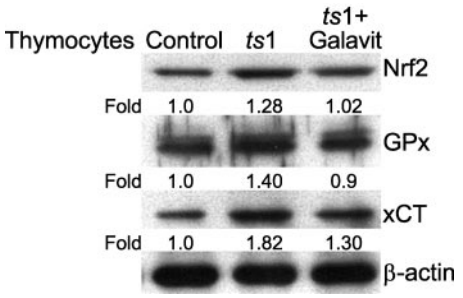

FIG. 8. GVT treatment suppresses elevation of Nrf2, GPx, and xCT in thymocytes from *ts*1-infected mice. Thymocytes were isolated from uninfected control, *ts*1-infected untreated, and *ts*1-infected GVT-treated mice at 30 days p.i., and lysates were prepared for immunoblotting using antibodies to Nrf2, GPx, and xCT. All blots were stripped and reimmunoblotted with anti-β-actin antibody as a protein-loading control. The results shown are representative of three independent experiments.

In Fig. 6C, which shows HE-stained thymus sections from control uninfected, *ts*1-infected, and *ts*1-infected GVT-treated mice (left to right, respectively), thymi from *ts*1-infected untreated mice showed dramatic atrophy by 30 days p.i., with collapse of the thymic lobules (Fig. 6C, compare middle and left panels). By contrast, sections of thymus from the *ts*1-infected GVT-treated mice (Fig. 6C) contained lobules of normal size, each with clear corticomedullary organization, although some cortical thinning was evident (compare left and right panels of bottom row, Fig. 6C).

GVT treatment increases levels of DNA synthesis in thymocytes from *ts*1-infected mice. Thymocytes from *ts*1-infected mice typically show depression of DNA synthesis (measured as [^{3}H]thymidine uptake) if they are isolated at 30 days p.i. (49). At that time, peripheral lymphocytes from *ts*1-infected mice also show depressed DNA synthesis relative to lymphocytes from uninfected animals (68). The depression of DNA synthesis seen in *ts*1-infected thymocytes thus reflects not only the generalized immunosuppression that follows *ts*1 infection (49), but also the death or functional inhibition of T-cell progenitors in infected mice.

To determine whether GVT treatment can restore normal levels of DNA synthesis and prevent the death of thymocytes of infected mice, we isolated thymocytes from uninfected control mice, uninfected GVT-treated mice, *ts*1-infected untreated mice, and *ts*1-infected GVT-treated mice at 30 days p.i. and measured their levels of DNA synthesis by pulsing them with [^{3}H]thymidine. The data in Fig. 7 show that while thymocytes from *ts*1-infected mice, as expected, had depressed DNA synthesis relative to thymocytes from uninfected mice, thymocytes taken from infected, GVT-treated mice showed normal levels of DNA synthesis. Interestingly, thymocytes from uninfected GVT-treated mice showed markedly increased DNA synthesis relative to thymocytes from untreated uninfected mice (Fig. 7). These results suggest that GVT is mitogenic for normal thymocytes from uninfected animals and that it restores normal levels of DNA synthesis in thymocytes from infected GVT-treated mice. In light of the extensive cell death occurring in thymi from untreated *ts*1-infected mice (Fig. 6C), we conclude that the normal DNA synthesis levels in thymocytes isolated from GVT-treated animals reflect protection of the cells by the drug.

GVT reverses *ts*1-associated upregulation of oxidative-stress markers in thymocytes. Earlier work from this laboratory established that *ts*1-infected cultured astrocytes show intracellular accumulation of gPr80^{env}, which is associated with oxidative and ER stress and depletion of GSH (24, 29, 45). These cells also have increased levels of markers of oxidative stress and exhibit elevated antioxidant defenses, including upregulated levels of Nrf2 and its downstream target proteins GPx and xCT, the cell surface cystine-glutamate antiporter (45). During these studies, we discovered that some infected astrocytes survive *ts*1 infection by mobilizing specific antioxidant defense pathways orchestrated by the transcription factor Nrf2 (46).

Accumulation of gPr80^{env} also occurs in *ts*1-infected thymocytes (18, 66). Given that GVT treatment decreases Nrf2 levels in *ts*1-infected astrocytes in vitro (Fig. 3), we asked whether GVT might also affect *ts*1-associated levels of Nrf2, GPx, or xCT in thymocytes from *ts*1-infected mice. The Western blotting data in Fig. 8 show that thymocytes from *ts*1-infected untreated mice show upregulated antioxidant defenses, as indicated by increased levels of Nrf2, GPx, and xCT relative to levels from uninfected mice at 30 days p.i. By contrast, none of these markers of oxidative stress is elevated in thymocytes from *ts*1-infected mice treated with GVT. Rather, the levels of Nrf2 and of its target gene products in these cells are similar to those of thymocytes from uninfected controls (Fig. 8).

GVT protection and effects on *ts*1 and WT virus titers in the CNS and thymus. *ts*1 shows enhanced replication in the CNS relative to its parent virus strain (WT), although titers of *ts*1 in the thymus are similar to those in mice infected with WT (66). Our recent published work suggests that the difference in CNS titers for *ts*1 and WT may be associated with higher H_2O_2 production elicited in these tissues by infection with *ts*1 (45,

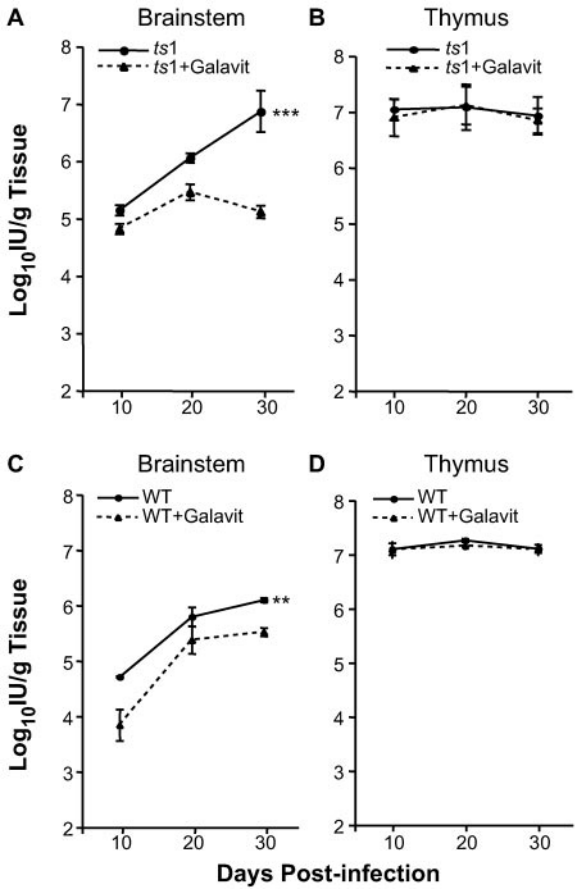

FIG. 9. Early GVT treatment (starting at 2 days p.i.) suppresses *ts*1 replication in the CNS, but not in the thymus. *ts*1 virus titers were determined at 10, 20, and 30 days p.i. for brainstem (A) and thymus (B) from *ts*1-infected untreated versus *ts*1-infected GVT-treated mice. WT virus titers were determined at 10, 20, and 30 days p.i. for brainstem (C) and thymus (D) tissues. The data points represent average viral titers for tissues from three to six mice, ± standard deviation, at each time point. **, $P < 0.01$. ***, $P < 0.001$.

65). Based on these findings, we hypothesized that GVT treatment might reduce CNS viral titers in *ts*1-infected mice more effectively than it does CNS titers in WT-infected mice. To assess whether *ts*1 replication is differentially affected by GVT treatment in the CNS or thymi of infected mice, we therefore compared the titers of *ts*1 in brainstem and thymus tissues of *ts*1-infected untreated or *ts*1-infected GVT-treated mice, and of WT-infected untreated versus WT-infected GVT-treated mice, at 10, 20, and 30 days p.i.

Figure 9A shows that the *ts*1 titers in the brainstems of *ts*1-infected untreated and *ts*1-infected GVT-treated mice were substantial and similar at 10 days p.i. but that this situation had changed markedly by 30 days p.i., at which time CNS tissues from GVT-treated mice contained much smaller amounts of virus (~50-fold less than *ts*1-infected untreated control CNS tissues). Figure 9C shows that GVT treatment also reduced WT titers in the CNS, but to a lesser extent than for *ts*1 titers (compare Fig. 9A to C). Notably, the virus titers from the thymi of the treated versus untreated *ts*1-infected animals were also high at 10 days p.i. and remained so for both groups of mice at all time points (Fig. 9B). Figure 9D shows that WT titers in the thymi from the treated versus untreated WT-infected mice remained high, with or without GVT treatment, at all time points, as in *ts*1-infected untreated and *ts*1-infected GVT-treated mice (compare Fig. 9B to D).

To determine whether the reduction of virus in the CNS was a result of direct antiviral activity of GVT, another set of animals was infected and either left untreated or treated with GVT beginning at 10 days p.i., rather than immediately after infection. Figure 10A shows that GVT treatment by this delayed schedule still prolonged survival after infection, although *ts*1 titers in the CNS of the infected untreated versus infected treated mice were similar at 30 days p.i. (Fig. 10B). These results show that GVT protection of the CNS can occur even under conditions where virus is replicating there, just as it can in the thymus.

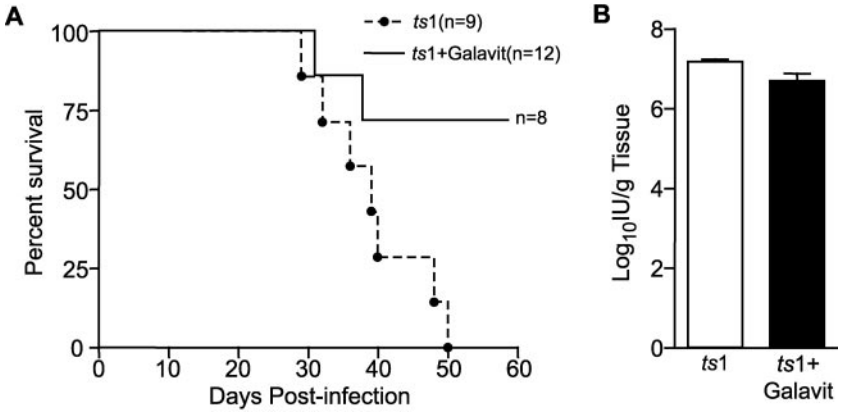

FIG. 10. Late GVT treatment (starting at 10 days p.i.) promotes survival in *ts*1-infected mice without reducing the virus titer in the CNS. Twenty-seven mice were infected with *ts*1 4 days after birth and then divided into two groups. Fifteen mice received intraperitoneal injections of GVT at 250 mg/kg of body weight/day for 5 days a week, starting at 10 days p.i. The remaining 12 received the same volume of 0.9% normal saline (infected untreated controls) using the same route and on the same schedule. At 30 days p.i., three mice from each group were sacrificed for brainstem *ts*1 titer determinations. Treatment was continued for the remaining mice for 5 days/week until 50 days p.i., at which time all of the mice in the untreated infected control group had died. At that time, 8 of the 12 GVT-treated mice were alive and asymptomatic (A). Survival curves for untreated infected versus infected mice treated with GVT starting at 10 days p.i. (B) Average brainstem virus titers, plus standard deviations, from three mice taken from the *ts*1-infected untreated group versus three mice taken from the infected GVT-treated group, whose survival curves appear in panel A.

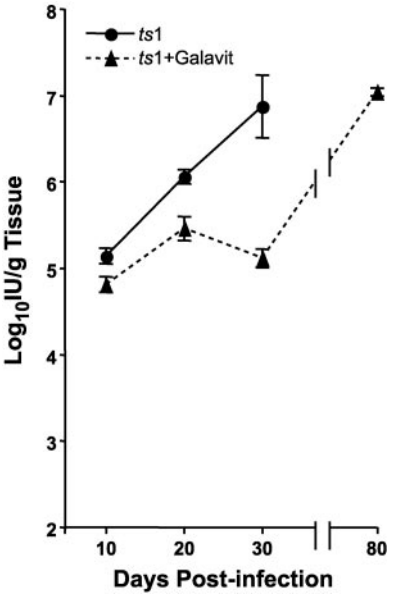

FIG. 11. *ts*1 replication resumes when GVT treatment is terminated. Brainstems were isolated from *ts*1-infected GVT-treated mice (early treatment protocol), and *ts*1 titers were determined at 10, 20, and 30 days p.i. GVT treatment was then terminated for the remaining mice in the infected treated group at 50 days p.i., and *ts*1 titers in their brainstem tissues were determined at 80 days p.i. Each point in the graph represents the average virus titer, ± standard deviation, for three to six mice.

Virus replication reemerges in the CNS when GVT treatment is stopped. The data in Fig. 4A show that GVT is neuroprotective for as long as it is administered, at an appropriate dosage, to infected mice. However, hindlimb paralysis and death eventually occur in all treated animals after GVT treatment is stopped. To find out whether the development of these symptoms coincides with rising viral titer in the CNS, we measured CNS brainstem viral titers at 80 days p.i. (30 days after cessation of GVT treatment), at which time the first symptoms of neuropathology appeared in this group. Figure 11 shows that the titers of *ts*1 in the brainstems of these GVT-terminated infected animals were comparable to the high levels of virus present in the brainstems of infected untreated mice at 30 days p.i.

Effects of early GVT treatment on *ts*1 replication and lipid peroxidation in brainstem and thymus of infected mice. One of best histochemically detectable markers of oxidative stress in tissues is MDA, which appears during lipid peroxidation of cell membranes (53, 59). After it is produced, MDA forms adducts with specific proteins in cells. To determine whether MDA adducts are present in increased amounts in cells of *ts*1-induced CNS spongiform lesions or in *ts*1-infected thymi, and to find out whether early GVT treatment affects the levels of this oxidative stress marker in either location in infected mice, brainstem and thymus sections were prepared from control uninfected, *ts*1-infected untreated, and *ts*1-infected GVT-treated mice at 30 days p.i. and stained both with antibody to viral gp70 and with antibody to MDA.

The data in Fig. 12 show groups of three photomicrographs (top, middle, and bottom rows), with each set of three showing the same field photographed under the bandpass filters for fluorescein isothiocyanate (left), for Texas Red (middle), and for both (detection of immunoreactive gp70 and MDA; right). The top horizontal row (control uninfected mouse brainstem) in Fig. 12A shows that neither gp70 nor MDA is present in CNS tissues from uninfected animals. The middle horizontal row of photomicrographs in Fig. 12A (*ts*1-infected untreated mouse) show that both gp70-reactive cells (left and right) and MDA adducts (middle and right) are abundant in spongiform lesions in the brainstems of *ts*1-infected untreated mice. The photomicrographs in the bottom horizontal row of Fig. 12A (*ts*1-infected GVT-treated mouse) show that while widely scattered, brightly stained, gp70-positive cells are present, these cells are few and far between, and spongiform lesions are absent. Also absent is any significant amount of immunodetectable MDA (middle and right), denoting suppression of brainstem lipid peroxidation (and oxidative stress) by GVT treatment given under these conditions.

The photomicrographs in Fig. 12B are configured in the same way as those in Fig. 12A, except that the tissue sections are from thymi of control uninfected (top horizontal row), *ts*1-infected untreated (middle horizontal row), and *ts*1-infected GVT-treated (bottom horizontal row) mice. Again, as expected, neither immunoreactive gp70 nor MDA is present in the thymus section from the control uninfected mouse (top row). By contrast, large amounts of immunoreactive gp70 (green) are present in thymus sections both from *ts*1-infected untreated and from *ts*1-infected GVT-treated mice (middle and bottom horizontal rows, right and left images in each row). This result is consistent with the virus titer data shown in Fig. 9, which also document no antiviral effect of GVT treatment in the thymus, despite protection of the thymus by the drug. Significantly, however, the untreated and *ts*1-infected GVT-treated sections differed in one important respect, which was that MDA protein adducts, reflecting ongoing oxidant stress, were abundant in the corticomedullary region of the infected untreated mouse thymus section (middle row, middle and right images) but present only at background levels in the section from the infected GVT-treated mouse (Fig. 12B, compare bottom horizontal row, middle and right images, with top horizontal row, middle and right images). These data suggest that GVT treatment protects the thymus by reducing oxidative stress, rather than by reducing *ts*1 replication.

DISCUSSION

Earlier work from this laboratory showed that damage to the CNS and thymus of infected mice is suppressed by treatment with the antioxidant NAC (35). However, while NAC eliminates thymic atrophy, it has relatively limited effects against neurodegeneration. This could be due to its limited ability to cross the blood-brain barrier (19, 41). We report here that treatment with another antioxidant, GVT, protects against neurodegeneration much more effectively than does NAC and that it prevents thymic atrophy and wasting for as long as treatment is administered and for up to 30 days after treatment is stopped. GVT also decreases intracellular H_2O_2 in PACs infected with *ts*1 in vitro, diminishes Nrf2 activation in infected PACs and in thymocytes isolated from *ts*1-infected mice, and reduces markers of lipid peroxidation in CNS and thymic tissues of *ts*1-infected mice. Since GVT is a reductant that re-

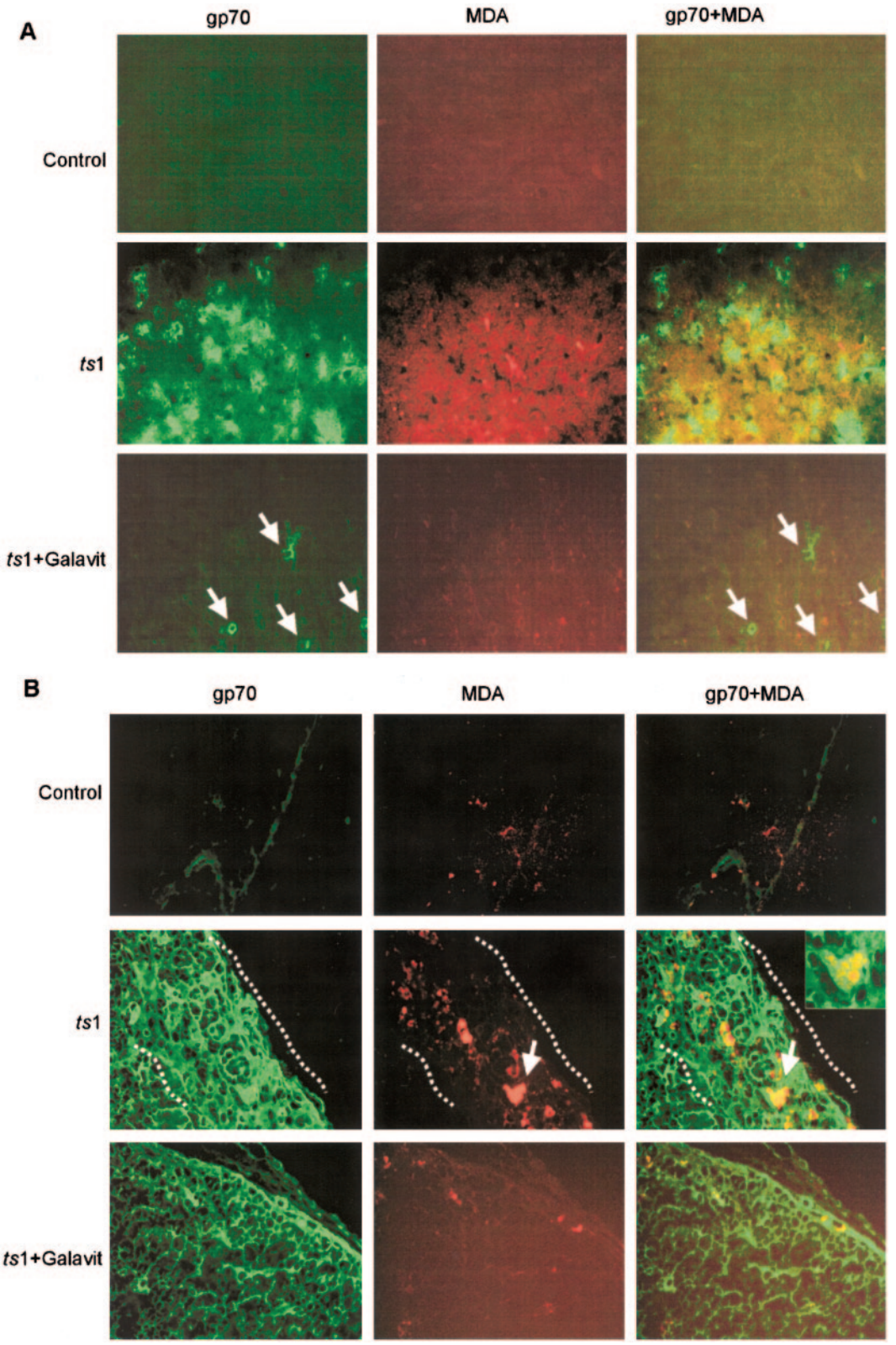

FIG. 12. Early GVT treatment protects the brainstem and the thymus from oxidative stress after *ts*1 infection, although it does not affect *ts*1 replication in the thymus. Brainstems and thymi from uninfected control mice, *ts*1-infected untreated mice, and *ts*1-infected GVT-treated mice were isolated and snap-frozen at 30 days p.i. Sections cut from these brainstems were then immunostained with fluorescently labeled antibody against gp70 (green) and MDA (red) to detect infection (gp70) and MDA-conjugated proteins (MDA), which are products of membrane lipid peroxidation in tissues undergoing oxidative stress. (A) Brainstem sections. (B) Thymus sections. Infected cells (green staining) and MDA adducts (red staining). In the left and right panels of the bottom row in panel A, which show a brainstem section from a GVT-treated *ts*1-infected mouse,

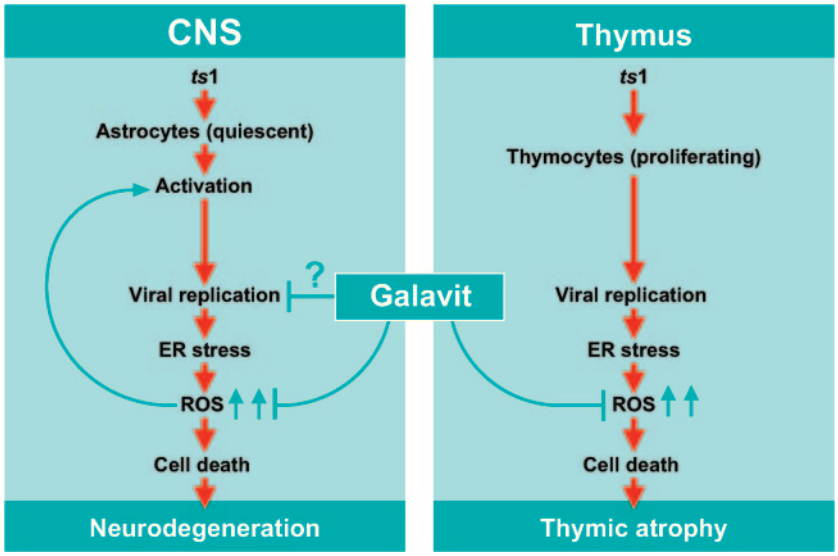

FIG. 13. Possible mechanisms for CNS and thymus protection by GVT. Productive infection by retroviruses generally requires that the target cells be activated. In the CNS, potential *ts*1 target cells (glial cells, including astrocytes) are quiescent, while *ts*1 target cells in the thymus (including thymocytes) are naturally proliferating cells. After *ts*1 inoculation, virus-induced oxidative stress events activate glial cells in the untreated CNS, allowing the virus to spread. If GVT is administered immediately after inoculation, its presence in the CNS may inhibit early cell activation events necessary for *ts*1 to replicate there. Even if virus infection is already established in the CNS, drug administration at a later time is still neuroprotective, although large amounts of replicating virus are present. Similarly, GVT protects the thymus from *ts*1-induced oxidative stress, thereby preserving the thymic cytoarchitecture and thymocyte cell division, without reducing *ts*1 replication. We propose that GVT protects the CNS and thymus against oxidative damage after *ts*1 infection and that this action of the drug is responsible for its neuroprotective and immunoprotective effects in *ts*1-induced neuroimmunodegeneration.

verses signs of oxidative damage in the CNS and in the thymus of *ts*1-infected mice, it seems likely that the mechanism for the drug's neuroimmunoprotection is based on its antioxidant effects. This idea received support from our recent studies showing that antioxidant defense mechanisms are activated in cultured astrocytes in response to their infection by *ts*1 (46) and that as many as half of these cells survive infection by successfully mobilizing these pathways (46).

GVT protection of *ts*1-infected mice is not associated with suppressed viral replication in the thymus. Similarly, GVT protection of infected mice is not associated with suppressed viral replication in the CNS if the drug is administered at 10 days p.i. It is noteworthy, however, that *ts*1 titers in the CNS are reduced, relative to those of untreated mice, if GVT is administered at earlier times after infection. This difference is likely to be due to the relatively quiescent state of CNS glial cells versus proliferative thymocytes in situ, since virus replication in cultured PACs (which are dividing cells) is only slightly reduced in the presence of GVT (data not shown) and not at all reduced in the CNS of mice receiving GVT beginning at 10 days p.i., by contrast to the reduction of *ts*1 titer in the CNS tissues of mice subjected to early-onset GVT treatment.

Although we cannot eliminate the possibility of a direct antiviral effect of GVT treatment in the CNS, the results reported here suggest that this is unlikely. The strongest argument against a direct antiviral effect comes from the events that follow termination of GVT treatment at the 250-mg/kg of body weight/day dose. When this treatment is stopped at 50 days p.i., all infected treated mice eventually become paralyzed and die, in association with rising CNS viral titers. These observations imply that GVT treatment does not eliminate the virus from the CNS but rather suppresses its replication there when GVT administration is begun immediately after infection. In addition, GVT increases [^{3}H]thymidine uptake and promotes DNA synthesis in thymocytes of *ts*1-infected mice, while allowing uninterrupted viral replication without cytopathic effects. If GVT were directly antiviral, it should not promote the survival and proliferation of cells productively infected with *ts*1. Another argument is that GVT reduces the CNS viral titer more effectively in *ts*1-infected mice than it does for WT virus-infected mice, indicating that GVT does not exert effects against the virus per se but on the different conditions generated and required by the two different viruses for replication (e.g., differing extents of ROS production in viral infection, as discussed above). Finally, as noted above, GVT reduces the viral titer in the CNS if administered early after infection, but not if treatment is started a few days later. Because the drug is neuroprotective in both contexts, we suggest

widely scattered, brightly stained gp70-positive (infected) cells are present (arrows), although spongiform lesions are absent. In the middle row in panel B, which shows a thymus section from an untreated *ts*1-infected mouse, the dotted lines bracket the cortex of one thymic lobule. In the middle and right panels of this row, an arrow identifies a group of cells in the cortex showing heavy red MDA staining, indicative of lipid peroxidation. This group of cells is magnified in the inset in the right panel of this row, where the cells are shown to be infected, as well (green gp70 staining). Magnification, (A) ×400; (B) ×400.

that GVT's antioxidant effects are responsible for its ability to prevent paralysis following *ts*1 infection.

The data presented here identify conditions (GVT treatment) under which the presence of a replication-competent cytopathic retrovirus causes neither acute neuropathological changes nor thymocyte death. Since GVT is an antioxidant, but not a direct antiviral agent, we propose that *ts*1-associated neuroimmunodegenerative disease is caused by oxidative stress resulting from virus infection, rather than from the viral load per se (33). Figure 13 is a schematic diagram that illustrates our hypothesized mechanisms for *ts*1 pathology and GVT's neuroimmunoprotection. The figure highlights the differential responses of the *ts*1 titer to GVT treatment in the CNS and thymus, while showing that *ts*1 pathology in both the CNS and thymus can be reversed by the antioxidant action of the drug.

Oxidative stress has been implicated in other retroviral neuroimmunodegenerative infections, such as HIV disease (15, 42, 47). In mice infected with the cytotoxic retrovirus PVC-211 MuLV, which also causes neurodegeneration similar to that following *ts*1 infection, antioxidant treatment attenuates oxidative-stress-induced neuropathology (61). In light of these examples, we propose that compounds with antioxidant properties, such as GVT, may be generally useful for the treatment of oxidative-stress-induced diseases, including HIV disease/AIDS, Alzheimer's disease, and ataxia telangiectasia.

ACKNOWLEDGMENTS

We thank Cynthia Kim, Lisa Whitson, Soojin Kim, Vanessa Edwards, and Shawna Johnson for their expert assistance in preparing the manuscript. We are also most grateful to Jodi M. Cahill and Lifang Zhang for providing invaluable technical assistance, to Kent Claypool for helping with flow cytometry analysis, and to Nancy Abbey and Jimi Lynn Brandon for preparing frozen sections and for advising us on immunohistochemical analyses.

This work was supported by NIH grants NS43984 and MH71583 (to Paul K.Y. Wong), NIEHS Center Grant ES07784, and Core Grant CA16672 and by funds from The Longevity Foundation in Austin, Texas.

REFERENCES

1. **Ball, J., J. A. McCarter, and S. M. Sunderland.** 1973. Evidence for helper independent murine sarcoma virus. I. Segregation of replication-defective and transformation-defective viruses. Virology **56:**268–284.
2. **Ball, J. K., T. Y. Huh, and J. A. McCarter.** 1964. On the statistical distribution of epidermal papillomata in mice. Br, J. Cancer **18:**120–123.
3. **Barlow, C., P. A. Dennery, M. K. Shigenaga, M. A. Smith, J. D. Morrow, L. J. Roberts II, A. Wynshaw-Boris, and R. L. Levine.** 1999. Loss of the ataxia-telangiectasia gene product causes oxidative damage in target organs. Proc. Natl. Acad. Sci. USA **96:**9915–9919.
4. **Bensaad, K., and K. H. Vousden.** 2005. Savior and slayer: the two faces of p53. Nat. Med. **11:**1278–1279.
5. **Betteridge, D. J.** 2000. What is oxidative stress? Metabolism **49:**3–8.
6. **Browne, S. E., L. J. Roberts II, P. A. Dennery, S. R. Doctrow, M. F. Beal, C. Barlow, and R. L. Levine.** 2004. Treatment with a catalytic antioxidant corrects the neurobehavioral defect in ataxia-telangiectasia mice. Free Radic. Biol. Med. **36:**938–942.
7. **Buhl, R., H. A. Jaffe, K. J. Holroyd, F. B. Wells, A. Mastrangeli, C. Saltini, A. M. Cantin, and R. G. Crystal.** 1989. Systemic glutathione deficiency in symptom-free HIV-seropositive individuals. Lancet **ii:**1294–1298.
8. **Butterfield, D. A., A. Castegna, C. M. Lauderback, and J. Drake.** 2002. Evidence that amyloid beta-peptide-induced lipid peroxidation and its sequelae in Alzheimer's disease brain contribute to neuronal death. Neurobiol. Aging **23:**655–664.
9. **Cerimele, F., T. Battle, R. Lynch, D. A. Frank, E. Murad, C. Cohen, N. Macaron, J. Sixbey, K. Smith, R. S. Watnick, A. Eliopoulos, B. Shehata, and J. L. Arbiser.** 2005. Reactive oxygen signaling and MAPK activation distinguish Epstein-Barr virus (EBV)-positive versus EBV-negative Burkitt's lymphoma. Proc. Natl. Acad. Sci. USA **102:**175–179.
10. **Chen, P., C. Peng, J. Luff, K. Spring, D. Watters, S. Bottle, S. Furuya, and M. F. Lavin.** 2003. Oxidative stress is responsible for deficient survival and dendritogenesis in purkinje neurons from ataxia-telangiectasia mutated mutant mice. J. Neurosci. **23:**11453–11460.
11. **Choe, W. K., G. Stoica, W. S. Lynn, and P. K. Y. Wong.** 1998. Neurodegeneration induced by MoMuLV-*ts*1 and increased expression of TNFα and Fas in the central nervous system. Brain Res. **779:**1–8.
12. **Ciriolo, M. R.** 2005. Redox control of apoptosis. Antioxid. Redox Signal **7:**432–435.
13. **Ciriolo, M. R., A. T. Palamara, S. Incerpi, E. Lafavia, M. C. Bue, P. De Vito, E. Garaci, and G. Rotilio.** 1997. Loss of GSH, oxidative stress, and decrease of intracellular pH as sequential steps in viral infection. J. Biol. Chem. **272:**2700–2708.
14. **Clark, S., J. Duggan, and J. Chakraborty.** 2001. *ts*1 and LP-BM5: a comparison of two murine retrovirus models for HIV. Viral Immunol. **14:**95–109.
15. **Eck, H. P., H. Gmunder, M. Hartmann, D. Petzoldt, V. Daniel, and W. Dröge.** 1989. Low concentrations of acid soluble thiol (cysteine) in the blood plasma of HIV-1 infected patients. Biol. Chem. Hoppe-Seyler **370:**101–198.
16. **Favier, A., C. Sappey, P. Leclerc, P. Faure, and M. Micoud.** 1994. Antioxidant status and lipid peroxidation in patients infected with HIV. Chem. Biol. Interact. **91:**165–180.
17. **Gil, L., G. Martinez, I. Gonzalez, A. Tarinas, A. Alvarez, A. Giuliani, R. Molina, R. Tapanes, J. Perez, and O. S. Leon.** 2003. Contribution to characterization of oxidative stress in HIV/AIDS patients. Pharmacol. Res. **47:** 217–224.
18. **Gonzales-Scarano, F., N. Nathanson, and P. K. Y. Wong.** 1995. Retroviruses and the nervous system, p. 409–490. *In* J. A. Levy (ed.), The Retroviridae, vol. 4. Plenum Press, New York, N.Y.
19. **Grinberg, L., E. Fibach, J. Amer, and D. Atlas.** 2005. *N*-Acetylcysteine amide, a novel cell-permeating thiol, restores cellular glutathione and protects human red blood cells from oxidative stress. Free Radic. Biol. Med. **38:**136–145.
20. **Halliwell, B.** 2001. Role of free radicals in the neurodegenerative diseases: therapeutic implications for antioxidant treatment. Drugs Aging **18:**685–716.
21. **Ito, K., A. Hirao, F. Arai, S. Matsuoka, K. Takubo, I. Hamaguchi, K. Nomiyama, K. Hosokawa, K. Sakurada, N. Nakagata, Y. Ikeda, T. W. Mak, and T. Suda.** 2004. Regulation of oxidative stress by ATM is required for self-renewal of haematopoietic stem cells. Nature **431:**997–1002.
22. **Itoh, K., N. Wakabayashi, Y. Katoh, T. Ishii, K. Igarashi, J. D. Engel, and M. Yamamoto.** 1999. Keap1 represses nuclear activation of antioxidant responsive elements by Nrf2 through binding to the amino-terminal Neh2 domain. Genes Dev. **13:**76–86.
23. **Kanno, T., E. E. Sato, S. Muranaka, H. Fujita, T. Fujiwara, T. Utsumi, M. Inoue, and K. Utsumi.** 2004. Oxidative stress underlies the mechanism for Ca^{2+}-induced permeability transition of mitochondria. Free Radic. Res. **38:**27–35.
24. **Kim, H. T., W. Qiang, N. Liu, V. L. Scofield, P. K. Y. Wong, and G. Stoica.** 2005. Up-regulation of astrocyte cyclooxygenase-2, CCAAT/enhancer-binding protein-homology protein, glucose-related protein 78, eukaryotic initiation factor 2 alpha, and c-Jun N-terminal kinase by a neurovirulent murine retrovirus. J. Neurovirol. **11:**166–179.
25. **Kroemer, G., and J. C. Reed.** 2000. Mitochondrial control of cell death. Nat. Med. **6:**513–519.
26. **Lee, J. M., M. J. Calkins, K. Chan, Y. W. Kan, and J. A. Johnson.** 2003. Identification of the NF-E2-related factor-2-dependent genes conferring protection against oxidative stress in primary cortical astrocytes using oligonucleotide microarray analysis. J. Biol. Chem. **278:**12029–12038.
27. **Limoli, C. L., R. Radoslaw, E. Giedzinski, S. Mantha, T. T. Huang, and J. R. Fike.** 2004. Cell-density-dependent regulation of neural precursor cell function. Proc. Natl. Acad. Sci. USA **101:**16052–16057.
28. **Lin, Y. C., C. W. Chow, P. H. Yuen, and P. K. Y. Wong.** 1997. Establishment and characterization of conditionally immortalized astrocytes to study their interaction with ts1, a neuropathogenic mutant of Moloney murine leukemia virus. J. Neurovirol. **3:**28–37.
29. **Liu, N., X. Kuang, H. T. Kim, G. Stoica, W. Qiang, V. L. Scofield, and P. K. Y. Wong.** 2004. Possible involvement of both endoplasmic reticulum- and mitochondria-dependent pathways in MoMuLV-*ts*1-induced apoptosis in astrocytes. J. Neurovirol. **10:**189–198.
30. **Liu, N., W. Qiang, X. Kuang, P. Thuillier, W. S. Lynn, and P. K. Y. Wong.** 2002. The peroxisome proliferator phenylbutyric acid (PBA) protects astrocytes from *ts*1 MoMuLV-induced oxidative cell death. J. Neurovirol. **8:**318–325.
31. **Liu, N., G. Stoica, M. Yan, V. L. Scofield, W. Qiang, W. S. Lynn, and P. K. Y. Wong.** 2005. ATM deficiency induces oxidative stress and endoplasmic reticulum stress in astrocytes. Lab. Invest. **85:**1471–1480
32. **Lombard, D. B., K. F. Chua, R. Mostoslavsky, S. Franco, M. Gostissa, and F. W. Alt.** 2005. DNA repair, genome stability, and aging. Cell **120:**497–512.
33. **Lynch, W. P., S. J. Robertson, and J. L. Portis.** 1995. Induction of focal spongiform neurodegeneration in developmentally resistant mice by implantation of murine retrovirus-infected microglia. J. Virol. **69:**1408–1419.
34. **Lynn, W. S., and P. K. Y. Wong.** 1995. Neuroimmunodegeneration: do

neurons and T cells utilize common pathways for cell death? FASEB J. **9:**1147–1156.
35. **Lynn, W. S., and P. K. Y. Wong.** 1998. Neuroimmunopathogenesis of *ts*1 MoMuLV infection. Neuroimmunomodulation **5:**248–260.
36. **Malorni, W., R. Rivabene, B. M. Lucia, R. Ferrara, A. M. Mazzone, R. Cauda, and R. Paganelli.** 1998. The role of oxidative imbalance in progression to AIDS: effect of the thiol supplier *N*-acetylcysteine. AIDS Res. Hum. Retrovir. **14:**1589–1596.
37. **Markesbery, W. R.** 1997. Oxidative stress hypothesis in Alzheimer's disease. Free Radic. Biol. Med. **23:**134–147.
38. **Mollace, V., H. S. Nottet, P. Clayette, M. C. Turco, C. Muscoli, D. Salvemini, and C. F. Perno.** 2001. Oxidative stress and neuroAIDS: triggers, modulators and novel antioxidants. Trends Neurosci. **24:**411–416.
39. **Nakamura, H., H. Masutani, and J. Yodoi.** 2002. Redox imbalance and its control in HIV infection. Antioxid. Redox Signal **4:**455–464.
40. **Nelyubov, M. V.** 2002. Cytokines in the pathogenesis of astrakhan spotted fever and North Asian scrub typhus: problems of immunocorrection. Bull. Exp. Biol. Med. **134:**165–167.
41. **Offen, D., Y. Gilgun-Sherki, Y. Barhum, M. Benhar, L. Grinberg, R. Reich, E. Melamed, and D. Atlas.** 2004. A low molecular weight copper chelator crosses the blood-brain barrier and attenuates experimental autoimmune encephalomyelitis. J. Neurochem. **89:**1241–1251.
42. **Ozdener, H.** 2005. Molecular mechanisms of HIV-1 associated neurodegeneration. J. Biosci. **30:**391–405.
43. **Peng, T. I., and J. T. Greenamyre.** 1998. Privileged access to mitochondria of calcium influx through *N*-methyl-D-aspartate receptors. Mol. Pharmacol. **53:** 974–980.
44. **Peterhans, E.** 1997. Oxidants and antioxidants in viral diseases: disease mechanisms and metabolic regulation. J. Nutr. **127:**962S–965S.
45. **Qiang, W., J. M. Cahill, J. Liu, X. Kuang, N. Liu, V. L. Scofield, J. R. Voorhees, A. J. Reid, M. Yan, W. S. Lynn, and P. K. Y. Wong.** 2004. Activation of transcription factor Nrf-2 and its downstream targets in response to Moloney murine leukemia virus *ts*1-induced thiol depletion and oxidative stress in astrocytes. J. Virol. **78:**11926–11938.
46. **Qiang, W., X. Kuang, J. Liu, N. Liu, V. L. Scofield, A. J. Reid, Y. Jiang, G. Stoica, W. S. Lynn, and P. K. Y. Wong.** 2006. Astrocytes survive chronic infection and cytopathic effects of retrovirus MoMuLV-*ts*1 by restoring thiol redox status via upregulation of antioxidant defenses. J. Virol. **80:**3273–3284.
47. **Roederer, M., F. J. Staal, H. Osada, and L. A. Herzenberg.** 1991. CD4 and CD8 T cells with high intracellular glutathione levels are selectively lost as the HIV infection progresses. Int. Immunol. **3:**933–937.
48. **Saha, K., and P. K. Y. Wong.** 1993. Rudimentary thymus of SCID mouse plays important role in the development of murine retrovirus-induced neurologic disorders. Virology **195:**211–218.
49. **Saha, K., P. H. Yuen, and P. K. Y. Wong.** 1994. Murine retrovirus-induced destruction of $CD4^+$ T cells and thymocytes are mediated through activation-induced death by apoptosis. J. Virol. **68:**2735–2740.
50. **Shikova, E., Y. C. Lin, K. Saha, B. R. Brooks, and P. K. Y. Wong.** 1993. Correlation of specific virus-astrocyte interactions and cytopathic effects induced by *ts*1, a neurovirulent mutant of Moloney murine leukemia virus. J. Virol. **67:**1137–1147.
51. **Smith, C. D., J. M. Carney, P. E. Starke-Reed, C. N. Oliver, E. R. Stadtman, R. A. Floyd, and W. R. Markesbery.** 1991. Excess brain protein oxidation and enzyme dysfunction in normal aging and in Alzheimer disease. Proc. Natl. Acad. Sci. USA **88:**10540–10543.
52. **Smith, M. A., G. Perry, P. L. Richey, L. M. Sayre, V. E. Anderson, M. F. Beal, and N. Kowall.** 1996. Oxidative damage in Alzheimer's. Nature **382:**120–121.
53. **Sonnerborg, A., G. Carlin, B. Akerlund, and C. Jarstrand.** 1988. Increased production of malondialdehyde in patients with HIV infection. Scand. J. Infect. Dis. **20:**287–290.
54. **Starkov, A. A., B. M. Polster, and G. Fiskum.** 2002. Regulation of hydrogen peroxide production by brain mitochondria by calcium and Bax. J. Neurochem. **83:**220–228.
55. **Stoica, G., E. Floyd, O. Illanes, and P. K. Y. Wong.** 1992. Temporal lymphoreticular changes caused by *ts*1, a paralytogenic mutant of Moloney murine leukemia virus-TB. Lab. Invest. **66:**427–436.
56. **Stoica, G., O. Illanes, S. I. Tasca, and P. K. Y. Wong.** 1993. Temporal central and peripheral nervous system changes induced by a paralytogenic mutant of Moloney murine leukemia virus TB. Lab Invest. **69:**724–735.
57. **Stoica, G., S. I. Tasca, and P. K. Y. Wong.** 2000. Motor neuronal loss and neurofilament-ubiquitin alteration in MoMuLV-*ts*1 encephalopathy. Acta Neuropathol. **99:**238–244.
58. **Szurek, P. F., P. H. Yuen, J. K. Ball, and P. K. Y. Wong.** 1990. A Val-25-to-Ile substitution in the envelope precursor polyprotein, $gPr80^{env}$, is responsible for the temperature sensitivity, inefficient processing of $gPr80^{env}$, and neurovirulence of *ts*1, a mutant of Moloney murine leukemia virus TB. J. Virol. **64:**467–475.
59. **Traverso, N., S. Menini, E. P. Maineri, S. Patriarca, P. Odetti, D. Cottalasso, U. M. Marinari, and M. A. Pronzato.** 2004. Malondialdehyde, a lipoperoxidation-derived aldehyde, can bring about secondary oxidative damage to proteins. J. Gerontol. A **59:**B890–B895.
60. **Viviani, B., E. Corsini, M. Binaglia, C. L. Galli, and M. Marinovich.** 2001. Reactive oxygen species generated by glia are responsible for neuron death induced by human immunodeficiency virus-glycoprotein 120 in vitro. Neuroscience **107:**51–58.
61. **Wilt, S. G., N. V. Dugger, N. D. Hitt, and P. M. Hoffman.** 2000. Evidence for oxidative damage in a murine leukemia virus-induced neurodegeneration. J. Neurosci. Res. **62:**440–450.
62. **Wong, P. K. Y., G. Prasad, J. Hansen, and P. H. Yuen.** 1989. *ts*1, a mutant of Moloney murine leukemia virus-TB, causes both immunodeficiency and neurologic disorders in BALB/c mice. Virology **170:**450–459.
63. **Wong, P. K. Y.** 1990. Moloney murine leukemia virus temperature-sensitive mutants: a model for retrovirus-induced neurologic disorders. Curr. Top. Microbiol. Immunol. **160:**29–60.
64. **Wong, P. K. Y., E. Floyd, and P. F. Szurek.** 1991. High susceptibility of FVB/N mice to the paralytic disease induced by *ts*1, a mutant of Moloney murine leukemia virus TB. Virology **180:**365–371.
65. **Wong, P. K. Y., C. Knupp, P. H. Yuen, M. M. Soong, J. F. Zachary, and W. A. F. Tompkins.** 1985. *ts*1, a paralytogenic mutant of MoMuLV-TB, has an enhanced ability to replicate in CNS and primary nerve cell culture. J. Virol. **55:**760–767.
66. **Wong, P. K. Y., W. S. Lynn, Y. C. Lin, W. Choe, and P. H. Yuen.** 1998. *ts*1 MoMuLV: a murine model of neuroimmunodegeneration, p. 75–93. *In* P. K. Y. Wong and W. S. Lynn (ed.), Neuroimmunodegeneration. R. G. Landes, Austin, Tex.
67. **Wong, P. K. Y., K. Saha, Y.-C. Lin, W. S. Lynn, and P. H. Yuen.** 1996. Long term cultivation and productive infection of primary thymocyte cultures by a thymocytopathic murine retrovirus. Virology **215:**203–206.
68. **Wong, P. K. Y., P. F. Szurek, E. Floyd, K. Saha, and B. R. Brooks.** 1991. Alteration from T to B cell tropism reduces thymic atrophy but not neurovirulence induced by *ts*1, a mutant of Moloney murine leukemia virus TB. Proc. Natl. Acad. Sci. USA **88:**8991–8995.
69. **Wong, P. K. Y., and P. H. Yuen.** 1994. Cell types in the central nervous system infected by murine retroviruses: implications for the mechanisms of neurodegeneration. Histol. Histopathol. **9:**845–848.
70. **Wright, B. S., P. A. O'Brien, G. P. Shibley, S. A. Mayyasi, and J. C. Lasfargues.** 1967. Infection of an established mouse bone marrow cell line (JLS-V9) with Rauscher and Moloney murine leukemia viruses. Cancer Res **27:**1672–1677.
71. **Yu, Y., W. Choe, G. Stoica, and P. K. Y. Wong.** 1997. Development of pathological lesions in the central nervous system of transgenic mice expressing the *env* gene of *ts*1 Moloney murine leukemia virus in the absence of the viral *gag* and *pol* genes and viral replication. J. Neurovirol. **3:**274–282.